

Improvement of Corrosion Resistance of Carbon Steel in Hydrochloric Acid Medium by 3,6-bis(3-Pyridyl)Pyridazine

F. Bentiss^{1,*}, M. Outirite², M. Traisnel², H. Vezin², M. Lagrenée², B. Hammouti³, S.S. Al-Deyab⁴, C. Jama²

¹ Laboratoire de Chimie de Coordination et d'Analytique (LCCA), Faculté des Sciences, Université Chouaib Doukkali, B.P. 20, M-24000 El Jadida, Morocco

² Université Lille Nord de France, F-59000 Lille, France

³ LCAE-URAC18, Faculté des Sciences, Université Mohammed Premier, B.P. 717, 60000 Oujda, Morocco

⁴ Petrochemical Research Chair, Department of Chemistry, College of Science, King Saud University, B.O. 2455, Riaydh 11451, Saudi Arabia

*E-mail: fbentiss@enscl.fr

Received: 17 December 2011 / Accepted: 18 January 2012 / Published: 1 February 2012

Corrosion inhibition of carbon steel in normal hydrochloric acid solution at 30°C by new pyridazine derivative, namely 3,6-bis(3-pyridyl) pyridazine (3-PYP) has been studied by a series of known techniques such as weight loss, polarisation and electrochemical impedance spectroscopy (EIS). The experimental results have showed that this organic compound revealed a good corrosion inhibition and that the inhibition efficiency is increased with the inhibitor concentration. Potentiodynamic polarisation suggested that it is a mixed type of inhibitor. Two time constants determined by the charge-transfer and the adsorption of the inhibitor, respectively, can be readily outlined. The adsorption of 3-PYP on the carbon steel surface, in 1 M HCl solution, obeyed to the Temkin's isotherm with a very high negative value of the standard Gibbs free energy of adsorption $\Delta G_{\text{ads}}^{\circ}$ (chemisorption). Quantum chemical calculations and X-ray photoelectron spectroscopy (XPS) analysis were carried out to establish the mechanism of corrosion inhibition of carbon steel in 1 M HCl medium in the presence of 3,6-bis(3-pyridyl)pyridazine (3-PYP).

Keywords: Pyridazine; Carbon steel; Acid solution; EIS; XPS; Acid inhibition

1. INTRODUCTION

Acid solutions are commonly used for the removal of undesirable scale and rust in the metal working, cleaning of boilers and heat exchangers. Hydrochloric acids are most widely used for all these purposes. However, the strong corrosivity of hydrochloric acid needs to be controlled by an

appropriate corrosion inhibitor [1-4]. Most well-known acid corrosion inhibitors are organic compounds containing nitrogen, sulfur, and oxygen atoms; nitrogen-containing organic compounds are known to be efficient corrosion inhibitors in hydrochloric acid solutions, while sulfur-containing compounds are sometimes preferred for sulphuric acid solutions [5]. Among them, N-heterocyclic compounds are considered to be the most effective corrosion inhibitors for steel in acid media [6,7]. They exert inhibition action through adsorption on the metal surface blocking the active sites by displacing water molecules and forming a compact barrier film to decrease the corrosion rate. The adsorption of N-heterocyclic inhibitor takes place through nitrogen heteroatom, as well as those with unsaturated bonds or aromatic rings in their molecular structures [8]. Generally, inhibition efficiency of N-heterocyclic organic inhibitor always increases with the number of aromatic systems and the availability of electronegative atoms in the molecule [9]. Many N-heterocyclic compounds, such as triazole derivatives [10-20], oxadiazole derivatives [21-30], thiadiazole derivatives [31-42], benzimidazole derivatives [43-45], pyrazole derivatives [46-49], purine derivatives [50-52], pyrimidine derivatives [53], quinoline derivatives [54], etc... have been used for the corrosion inhibition of iron or steel in acidic media. A survey of literature reveals that little attention has been paid on the use of pyridazine derivatives in the inhibition of steel corrosion. Indeed, the use of the newly synthesised pyridazine derivatives; 5-benzyl-6-methyl pyridazine-3-thione and 5-benzyl-6-methyl pyridazine-3-one; on the inhibition of pure iron in 1 M HCl have been investigated for the first time by Chetouani et al. in 2002 [55]. Their results showed that these pyridazine derivatives are efficient inhibitors and act essentially as cathodic-type inhibitors. This work was subsequently extended to study the relation between molecular structure of these pyridazines and their inhibitive action [56]. In 2004, Bouklah et al. studied the effect of the substitution of an oxygen atom by sulphur in a pyridazinic molecule towards inhibition of corrosion of steel in 0.5 M H₂SO₄ medium [57]. They showed that the presence of a sulphur atom considerably increased the inhibition efficiency. Afterwards, the Hammouti group investigated the use of some pyridazine derivatives, namely 5-(2-chlorobenzyl)-6-methylpyridazine-3(2H)-thione (P1) and 5-(4-chlorobenzyl)-6-methylpyridazine-3(2H)-thione (P2), as potential inhibitors in the steel corrosion in 0.5 M H₂SO₄ [58]. The obtained results showed that the inhibition efficiency of P1 increases with the increase of concentration to reach about 99% at 0.5 mM and the ability of the molecule to adsorb on the steel surface was dependent on the position of the chloride atom on the benzyl substituent. In the same acid medium (0.5 M H₂SO₄), the study of inhibition effect of diethyl pyrazine-2,3-dicarboxylate on the corrosion steel revealed that this pyridazine derivative is not efficient for above purpose [59-60]. In this field, we have previously reported that the 1,4-bis(2-pyridyl)-5H-pyridazino[4,5-b]indole (PPI) is a good corrosion inhibitor for carbon steel in 1 M HCl medium [61]. X ray photoelectron spectroscopy (XPS) and theoretical calculation were carried out to establish the mechanism of corrosion inhibition using PPI inhibitor. Recently, Deng et al. investigated the inhibition effect of two pyrazine derivatives, 2-aminopyrazine (AP) and 2-amino-5-bromopyrazine (ABP), on the corrosion of cold rolled steel (CRS) in 1 M hydrochloric acid [62]. These two pyrazine derivatives act as good inhibitors and the maximum of inhibition efficiency values are 95.1% (AP) and 97.4% (ABP) at 1.0 mM.

In continuation of our work on development of pyridazine derivatives as corrosion inhibitors in acidic media [57,61], we studied the corrosion inhibiting behaviour of a novel synthesised pyridazine

derivative, namely 3,6-bis(3-pyridyl)pyridazine (3-PYP), on carbon steel in 1 M HCl medium at 30°C. The choice of this compound was based on molecular structure considerations; i.e., 3-PYP has an ideal planar structure and the presence of four heteroatoms (nitrogen) and aromatic rings is known to facilitate the adsorption of molecule on the metal surface. Weight loss measurements, linear polarisation resistance, Tafel polarisation and electrochemical impedance spectroscopy (EIS) techniques were used to evaluate the inhibition properties of 3-PYP. Adsorption isotherm, Density Functional Theory (DFT) method and X-ray photoelectron spectroscopy (XPS) have been applied to study the mechanism of steel corrosion inhibition of this organic compound in acidic medium.

2. EXPERIMENTAL DETAILS

2.1. Materials

The tested inhibitor, namely 3,6-bis(3-pyridyl)pyridazine (3-PYP), was synthesised according to a previously described experimental procedure [63]. The molecular structure of 3-PYP is shown in Figure 1. The structure of the 3-PYP was confirmed by ^1H and ^{13}C NMR, mass spectroscopy and elemental analysis.

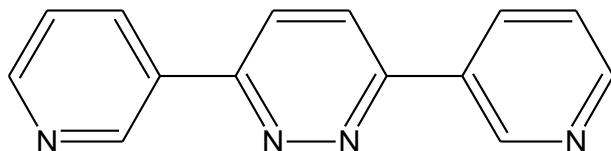


Figure 1. Chemical structure of the investigated 3,6-bis(3-pyridyl)pyridazine (3-PYP).

3-PYP: Yield 57.6%; mp 210°C; ^1H -NMR (dimethyl- d_6 sulfoxide; 300 MHz): δ (ppm) 7.64 (m, 2H); 8.21 (s, 2H); 8.44 (t, 2H); 8.89 (t, 2H), 9.35 (s, 2H); ^{13}C -NMR (dimethyl- d_6 sulfoxide; 75 MHz): δ (ppm) 123.92, 126.71, 130.55, 134.39, 146.36, 161.12, 165.81; MALDI-TOFMS: m/z 235 ($M+1$). Anal. Calcd for $\text{C}_{14}\text{H}_{10}\text{N}_4$: C, 71.78; H, 4.30; N, 23.92. Found: C, 71.56; H, 4.53; N, 23.68.

The concentration range of 3-PYP employed was 0.2 mM to 1.2 mM in order to compare their corrosion inhibition properties with those of similar heterocyclic compounds.

The material used in this study is a carbon steel (Euronorm: C35E carbon steel and US specification: SAE 1035) with a chemical composition (in wt%) of 0.370 % C, 0.230 % Si, 0.680 % Mn, 0.016 % S, 0.077 % Cr, 0.011 % Ti, 0.059 % Ni, 0.009 % Co, 0.160 % Cu and the remainder iron (Fe). The steel samples were pre-treated prior to the experiments by grinding with emery paper SiC (120, 600 and 1200); rinsed with distilled water, degreased in acetone in an ultrasonic bath immersion for 5 min, washed again with bidistilled water and then dried at room temperature before use. The acid solutions (1 M HCl) were prepared by dilution of an analytical reagent grade 37 % HCl with doubly distilled water.

2.2 Corrosion tests

Weight loss, potentiodynamic polarisation, linear polarisation resistance (LPR) and electrochemical impedance spectroscopy (EIS) are four classical techniques which were used to determine the corrosion inhibitor characteristics of 3-PYP in 1 M HCl.

The gravimetric measurements were carried out at the definite time interval of 24 h at room temperature ($30 \pm 1^\circ\text{C}$) using an analytical balance (precision ± 0.1 mg). The steel specimens used have a rectangular form (length = 3 cm, width = 1.5 cm, thickness = 0.3 cm). Gravimetric experiments were carried out in a double glass cell equipped with a thermostated cooling condenser containing 100 ml of non-de-aerated test solution. After immersion period, the steel specimens were withdrawn, carefully rinsed with bidistilled water, ultrasonic cleaning in acetone, dried at room temperature and then weighted. Duplicate experiments were performed in each case and the mean value of the weight loss is calculated.

Linear polarisation resistance (LPR) and potentiodynamic polarisation measurements were performed in a conventional three-electrode cylindrical Pyrex glass cell. The temperature is thermostatically controlled. Pure carbon steel specimen was used as the working electrode, a platinum electrode as the counter electrode and a saturated calomel electrode (SCE) as the reference electrode. The working electrode (WE) in the form of disc cut from steel has a geometric area of 1 cm^2 and is embedded in polytetrafluoroethylene (PTFE). A fine Luggin capillary was placed close to the working electrode to minimize IR drop. All test solutions were de-aerated in the cell by using pure nitrogen for 10 min prior to the experiment. During each experiment, the test solution was mixed with a magnetic stirrer and the gas bubbling was maintained. Solartron Instruments SI 1287 potentiostat monitored by a personal computer via a GPIB Interface and CorrWarr2.80 software were used to run the tests and to collect the experimental data. Before each Tafel experiment, the carbon steel electrode was pre-polarised at $-800\text{ mV}_{\text{SCE}}$ for 10 min and thereafter the WE was allowed to corrode freely and its open circuit potential (OCP) was recorded as a function of time up to 1 h, the time necessary to reach a quasi-stationary value for the open-circuit potential. This steady-state OCP corresponds to the corrosion potential (E_{corr}) of the WE. For LPR measurements, the WE was polarised only in the range $\pm 20\text{ mV}$ vs. E_{corr} at a scan rate of 0.125 mV s^{-1} . After studying the open circuit potential and LPR tests, the potentiodynamic Tafel measurements were scanned from cathodic to the anodic direction, $E = E_{\text{corr}} \pm 200\text{ mV}$, with a scan rate of 0.5 mV s^{-1} . The Tafel and LRP data were analysed and fitted using the polarisation CorrView 2.80 software (Scribner Associates, Inc.).

Ac impedance tests were performed in a polymethyl methacrylate (PMMA) cell with a capacity of 1000 ml at $30 \pm 1^\circ\text{C}$, using a thermostat. A saturated calomel electrode (SCE) was used as the reference; while a platinum leaf was used as a counter electrode. All potentials are reported vs. SCE. The working electrode was prepared from a square sheet of carbon steel such that the area exposed to solution was 7.55 cm^2 . The impedance spectra were recorded 24 h after the exposure of the working electrode to the solution (no deaeration, no stirring). Ac impedance measurements were performed using a potentiostat Solartron SI 1287 and a Solartron 1255B frequency response analyzer and ZPlot 2.80 software was used to run the tests and to collect the experimental data. The response of the electrochemical system to ac excitation with a frequency ranging from 10^5 Hz to 10^{-2} Hz and peak to

peak amplitude of 10 mV was measured with data density of 10 points per decade. All EIS diagrams were recorded at the open circuit potential, i.e., at the corrosion potential E_{corr} . The duration of one EIS experiment was about 10 min. The impedance data were analysed and fitted with the simulation ZView 2.80, equivalent circuit software.

2.3. X-ray photoelectron spectroscopy (XPS)

The studied samples for X-ray photoelectron spectroscopy (XPS) before and after immersion in 1 M HCl medium were prepared by the same procedure as for the gravimetric test with carbon steel disk (1 cm²). After 24 h of immersion, the carbon steel sheet was rinsed with acetone and ultra pure water. X-ray photoelectron spectroscopy (XPS) spectra were recorded by a VG ESCALAB 220 XL spectrometer. The monochromatized Al-K α X-ray source ($h\nu = 1486.6$ eV) was operated in the CAE (constant analyser energy) mode (CAE = 150 eV for survey spectra and CAE = 30 eV for high resolution spectra), using the electromagnetic lens mode. The binding energy scale was initially calibrated using the Cu 2p_{3/2} (932.7 eV), Ag 3d_{5/2} (368.2 eV) and Au 4f_{7/2} (84 eV) peak positions, and internal calibration was referenced to the C 1s energy at 285 eV for aliphatic like species. Quantification of outer layers atomic composition was achieved using the software provided by VG Scientific. XPS spectra were deconvoluted using a non-linear least squares algorithm with a Shirley base line and a Gaussian–Lorentzian combination. XPS Peak-Fit 4.1 software was used for all data processing.

2.4. Computational method

All calculations were performed by means of the Gaussian 03 program on 18 processors Linux Transtec Cluster with parallel G03 Linda version. The molecular structure of 3-PYP was fully and geometrically optimised using the functional hybrid B3LYP Density Functional Theory formalism (DFT) and the 6-31G+ (2d,2p) orbital basis set for all atoms. Self Consistent Reaction Field (SCRF) calculations in consideration of the solvent effect were done using the Polarized Continuum Method (PCM) with UAHF set of radii for standard solvent with water as solvent. The pK_a calculation was performed with the SPARC on line calculator.

3. RESULTS AND DISCUSSION

3.1. Corrosion inhibition evaluation

3.1.1. Gravimetric study

The effect of addition of different concentrations of 3-PYP on the corrosion of carbon steel in 1 M HCl solution was studied by weight loss measurements at 30 °C after 24 h of immersion period. For

every concentration, the mean value of the corrosion rate C_R ($\text{mg cm}^{-2} \text{h}^{-1}$) was determined and the inhibitor efficiency, $\eta_{\text{WL}}(\%)$, was calculated using Eqs. 1 and 2, respectively [64]:

$$C_R = \frac{W_b - W_a}{At} \quad (1)$$

$$\eta_{\text{WL}}(\%) = \left(1 - \frac{w_i}{w_0}\right) \times 100 \quad (2)$$

where W_b and W_a are the specimen weight before and after immersion in the tested solution, w_0 and w_i are the values of corrosion weight losses of carbon steel in uninhibited and inhibited solutions, respectively, A the area of the carbon steel specimen (cm^2) and t is the exposure time (h).

The values of percentage inhibition efficiency, $\eta_{\text{WL}}(\%)$, and corrosion rate (C_R) obtained from weight loss method at different concentrations of 3-PYP are summarized in Table 1. It is very clear that the 3-PYP inhibits the corrosion of carbon steel in 1 M HCl solution, at all concentrations used in this study, while the corrosion rate (C_R) decreases continuously with increasing additive concentration at 30°C; the maximum $\eta_{\text{WL}}(\%)$ of 92.8 % is achieved at 1.2 mM. The high inhibitive performance of 3-PYP suggests a strong bonding of this pyridazine derivative on the metal surface due to presence of several lone pairs from heteroatom (nitrogen) and π -orbitals, blocking the active sites and therefore decreasing the corrosion rate. However, the studies of the improvement of the corrosion resistance of carbon steel in 1 M HCl by other 3-pyridyl substituted 1,2,4 and 1,3,4-thiadiazoles and oxadiazoles, previously described in the same conditions, shows that the inhibition efficiency attains 98.3 % at 1.2 mM in the case of 2,5-bis(3-pyridyl)-1,2,4-thiadiazole (3-PTHD) [34], 96.8 % in the presence of 3,5-bis(3-pyridyl)-1,3,4-thiadiazole (3-PTH) [32] and 97.4 % in the case of 3,5-bis(3-pyridyl)-1,2,4-oxadiazole (3-DPOX) [30]. This behaviour can be explained by the presence of another heteroatom; sulfur in the case of thiadiazole or oxygen in the case of oxadiazole.

Table 1. Corrosion parameters obtained from weight loss measurements for carbon steel in 1 M HCl containing various concentrations of 3-PYP at 30°C.

Conc. of inhibitor (mM)	C_R ($\text{mg cm}^{-2} \text{h}^{-1}$)	η_{WL} (%)
Blank	2.78	—
0.2	0.35	87.4
0.4	0.27	90.3
0.8	0.24	91.4
1.2	0.20	92.8

3.1.2. Polarisation studies

The aim of these investigations was to determine the influence of 3-PYP on the electrochemical behaviour of carbon steel in 1 M HCl. Polarisation curves of the carbon steel electrode in 1 M HCl

without and with addition of various concentrations of 3-PYP are shown in Fig. 2. As it can be seen, the anodic and cathodic reactions are affected by the addition of pyridazine derivative. Meaning that, the addition of 3-PYP to HCl solution reduces the anodic dissolution of steel and also retards the cathodic hydrogen evolution reaction. The inhibiting effect of 3-PYP may be related to its adsorption and formation of a barrier film on the electrode surface. These results indicated that this organic inhibitor exhibit cathodic and anodic inhibition effects. Therefore, 3-PYP can be classified as an inhibitor of relatively mixed effect (anodic/cathodic inhibition) in 1 M HCl.

Besides, the recorded polarisation curves in the presence of 3-PYP (Fig. 2) are characterized by the presence of anodic breakdown potential, E_b . This is the potential at which sudden rise in current density takes place. As a result, the surface film is shifted from stable to unstable state. As the concentration of inhibitor increased, E_b shifted to noble direction. The noble shift of E_b with increasing 3-PYP concentration reflected the increased adsorption of inhibitor on the metal surface. The noble shift of E_b and the decrease of the corresponding current densities with increasing the studied pyridazine concentration reflected the formation of anodic protective film on the electrode surface [20,65]. However, for potential higher than -300 mV_{SCE}, the presence of 3-PYP did not change the current-vs.-potential characteristics (Fig. 2). This potential can be defined as the desorption potential. The phenomenon may be due to the obvious metal dissolution, which led to a desorption of the inhibitor molecule from the electrode surface, in this case the desorption rate of the inhibitors is higher than its adsorption rate, so the corrosion current obviously increased with rising potential [66].

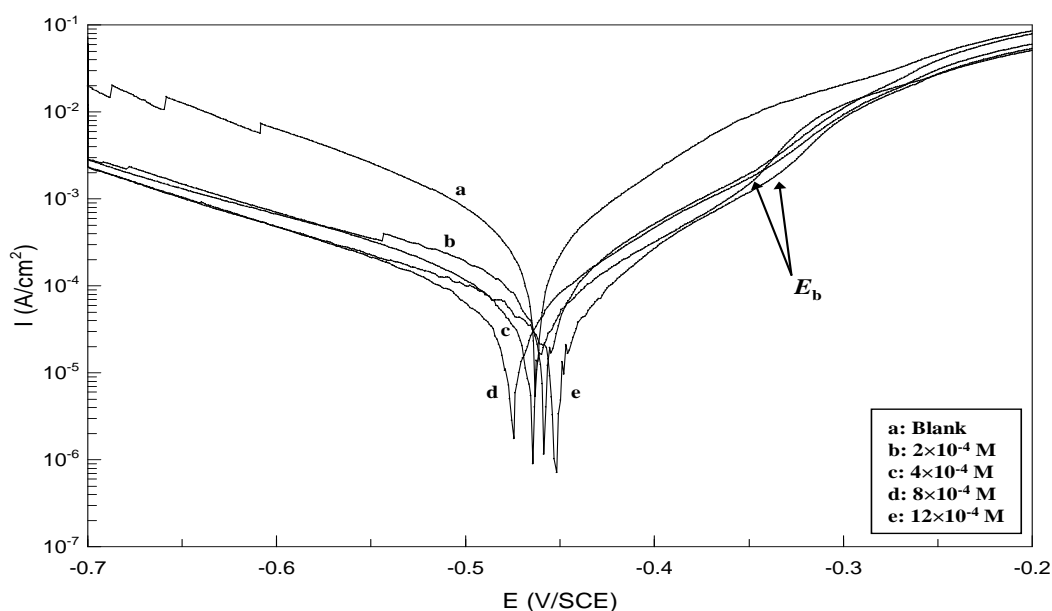


Figure 2. Polarisation curves for carbon steel in 1 M HCl containing different concentrations of 3-PYP.

Table 2 shows the electrochemical corrosion kinetic parameters, i.e. corrosion potential (E_{corr}), corrosion current density (j_{corr}), cathodic and anodic Tafel slopes (β_c , β_a), obtained from the extrapolation of the polarisation curves. The data were fitted using non-linear least square algorithm

based on the Tafel-LEV (Levenberg–Marquardt) method used along with CorrView 2.80 software. Table 2 also included percentage inhibition efficiency, η_{Tafel} (%) that was calculated from the following equation [20]:

$$\eta_{\text{Tafel}}(\%) = \frac{j_{\text{corr}} - j_{\text{corr}(i)}}{j_{\text{corr}}} \times 100 \quad (3)$$

where j_{corr} and $j_{\text{corr}(i)}$ are the corrosion current densities for steel electrode in the uninhibited and inhibited solutions, respectively. From the same Tafel polarisation curves, using only the range ± 20 mV vs. E_{corr} , the dc polarisation resistance (R_p) was evaluated and the R_p fit was obtained with a good correlation coefficient. The corresponding R_p values of carbon steel in 1 M HCl in the presence and absence of different concentrations of 3-PYP are given in Table 2. In addition, the R_p values obtained from the LPR experiment are also presented in Table 2. The LPR experiments were carried out in order to exclude the influence of the surface changes which may occur during polarisation at higher overpotentials in the case of potentiodynamic polarisation method. The good coincidence between the values of the polarisation resistance obtained by the two methods – polarisation resistance and polarisation curves, shows that no significant surface changes occur during the polarisation measurements at ± 200 mV vs. E_{corr} . The polarisation resistance (R_p) obtained by LPR method is used to calculate the corrosion current (j_{corr}) based on the Stern–Geary kinetics equation [67]. Inhibition efficiency, $\eta_{\text{LPR}}(\%)$, is calculated from R_p using the following equation:

$$\eta_{\text{LPR}}(\%) = \frac{R_{p(i)} - R_p}{R_{p(i)}} \times 100 \quad (4)$$

where R_p and $R_{p(i)}$ are the polarisation resistance of carbon steel electrode in the uninhibited and inhibited solutions, respectively.

Table 2. Polarisation parameters and the corresponding inhibition efficiency for the corrosion of carbon steel in 1 M HCl containing different concentrations of 3-PYP at 30°C.

Inhibitor Conc. (mM)	Tafel						LPR	
	E_{corr} vs SCE (mV)	j_{corr} ($\mu\text{A cm}^{-2}$)	β_a (mV dec ⁻¹)	β_c (mV dec ⁻¹)	R_p	η_{Tafel} (%)	R_p ($\Omega \text{ cm}^2$)	η_{LPR} (%)
Blank	-463	413	87.9	114.1	45.6.0	—	40.3	—
0.2	-458	110	91.1	142.1	203.6	73.4	192.2	79.0
0.4	-464	68	84.5	128.9	302.8	83.5	305.2	86.8
0.8	-476	65	87.3	141.4	351.9	84.3	343.1	88.3
1.2	-452	53	76.9	152.6	373.1	87.2	365.0	88.9

From Table 2, it is clear that the values of R_p increase and j_{orr} values decrease considerably with the increase of the concentration of 3-PYP, however, there is no definite trend in the shift of E_{corr} values with concentration. The values of the slopes of the anodic Tafel lines, β_a , show a slight change with the addition of 3-PYP suggesting that this studied inhibitor was first adsorbed onto the metal surface and impeded by merely blocking the reaction sites of the metal surface without affecting the anodic reaction mechanism [68]. However, β_c values for 3-PYP are higher than those for uninhibited solution. This increased value of β_c suggests that mechanism of hydrogen evolution reaction was changed in the presence of 3-PYP. This may probably be due to a diffusion or barrier effect [67]. According to Bockris and Srinivasan [69], this behaviour can be correlated to the decrease of the cathodic transfer coefficient which, in this case, can be ascribed to the thickening of the electric double layer due to the adsorbed inhibitor molecules.

The inhibition efficiency, $\eta(\%)$, calculated by both methods (LPR and potentiodynamic polarisation) shows the same trend (Table 2) and increases with 3-PYP concentration, reaching its maximum value at 1.2 mM. The polarisation data confirm the gravimetric results (3-PYP is a good inhibitor and depends on the inhibitor concentration) giving more detailed information about the inhibitor action of the 3-PYP. The differences observed between the two types of experiments (Tables 1 and 2) are probably due to a greater extent to the different exposure time in the corrosive solution.

3.1.3. Ac impedance study

An impedance measurement is a veritable tool and has been widely used in investigating corrosion inhibition processes. It provides information on both the resistive and capacitive behaviour at interface and makes it possible to evaluate the performance of the tested compounds as possible inhibitors against metals' corrosion. Impedance measurements of the carbon steel electrode at its open circuit potential after 24 h of immersion in 1 M HCl solution alone and in the presence of the studied pyridazine derivative were performed over the frequency range from 100 kHz to 10 mHz. The recorded EIS spectrum for carbon steel in 1 M HCl, Fig. 3, shows only one depressed capacitive loop at the higher frequency range (HF) with one capacitive time constant in the Bode-phase plot. In this case, the standard Randles' circuit model of Fig. 4a, which has been previously used [30], fits well our experimental results. In this equivalent circuit, R_s is the solution resistance, R_{ct} present the charge transfer resistance whose value is a measure of electron transfer across the surface and CPE is the constant phase element. The constant phase element, CPE, is introduced in the circuit instead of a pure double layer capacitor in order to take into account the electrode surface heterogeneity resulting from surface roughness, impurities, dislocations, grain boundaries, adsorption of inhibitors, formation of porous layers [70,71] and therefore to give a more accurate fit [72]. The impedance of the CPE is expressed as:

$$Z_{\text{CPE}} = A^{-1} (i\omega)^{-n} \quad (5)$$

where A is the magnitude of CPE (in $\Omega^{-1} s^n cm^{-2}$), ω is the sine wave modulation angular frequency (in $rad s^{-1}$), $i^2 = -1$ is the imaginary number, and n is an empirical exponent ($0 \leq n \leq 1$) which measures the deviation from the ideal capacitive behaviour [73,74]. The corresponding fitting results are listed in Table 3. In this table are also shown the calculated double layer capacitance (C_{dl}) derived from the CPE parameters according to the equation [75]:

$$C_{dl} = (A_d R_{ct}^{1-n_d})^{1/n_d} \tag{6}$$

and the relaxation time constant (τ_d) of charge-transfer process using the equation [75]:

$$\tau_d = C_{dl} R_{ct} \tag{7}$$

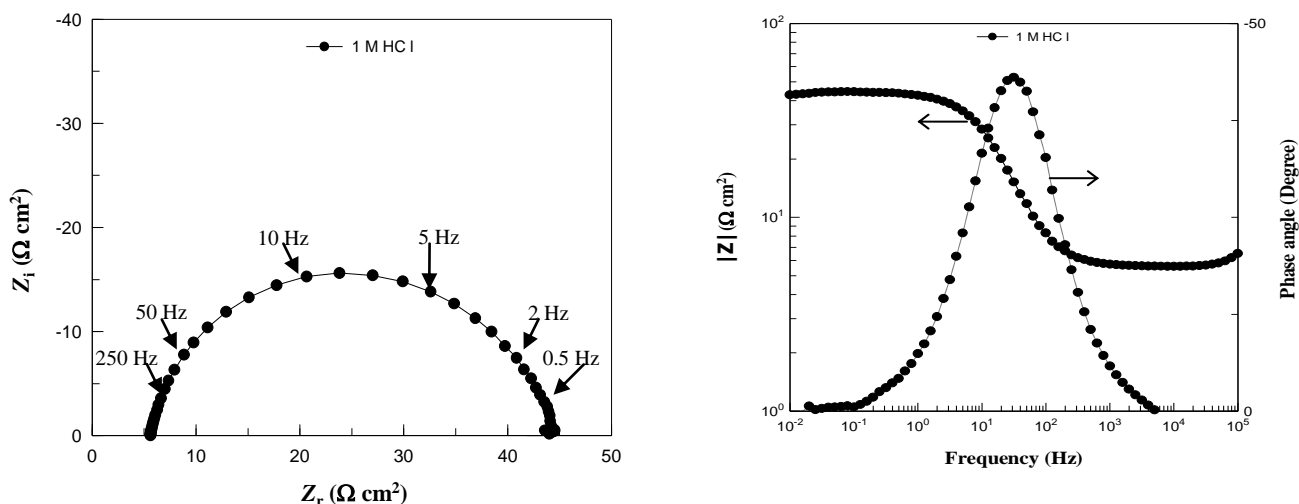


Figure 3. Nyquist and Bode diagrams for carbon steel in 1 M HCl after 24 h of immersion period at 30°C.

Table 3. Impedance parameters and inhibition efficiency values for carbon steel after 24 h immersion period in 1 M HCl containing different concentrations of 3-PYP at 30°C.

Conc. (mM)	R_s (Ωcm^2)	R_{ct} (Ωcm^2)	$10^4 A_d$ ($\Omega^{-1} s^n cm^{-2}$)	n_d	C_d ($\mu F cm^{-2}$)	τ_d (s)	R_a (Ωcm^2)	$10^4 A_a$ ($\Omega^{-1} s^n cm^{-2}$)	n_a	C_a (mF cm^{-2})	τ_a (s)	R_{pt} (Ωcm^2)	η_z (%)
Blank	5.70 ± 0.02	37.05 ± 0.13	8.44 ± 0.09	0.879 ± 0.001	52	0.0194	—	—	—	—	—	37.05 ± 0.13	—
0.2	6.30 ± 0.02	200.1 ± 1.6	1.35 ± 0.02	0.891 ± 0.002	87	0.0174	151.2 ± 2.6	41.04 ± 1.24	0.58 ± 0.01	2.92	0.440	351.3 ± 4.2	89.5
0.4	6.28 ± 0.01	239.6 ± 4.4	1.14 ± 0.01	0.901 ± 0.002	77	0.0183	161.7 ± 5.8	27.70 ± 1.42	0.57 ± 0.02	1.50	0.243	401.3 ± 10.2	90.8
0.8	7.60 ± 0.01	279.4 ± 6.4	0.99 ± 0.01	0.927 ± 0.002	74	0.0215	173.6 ± 7.8	20.28 ± 1.21	0.60 ± 0.02	1.12	0.194	464.8 ± 14.2	92.0
1.2	6.37 ± 0.01	312.4 ± 7.2	1.01 ± 0.01	0.905 ± 0.002	70	0.0220	181.0 ± 8.6	19.44 ± 1.41	0.57 ± 0.02	0.88	0.158	493.4 ± 15.8	92.5

Fig. 5 shows Nyquist plots and the representative Bode diagrams for carbon steel in 1 M HCl in the presence of various concentration of 3-PYP. The addition of 3-PYP to the aggressive solution leads

to a change of the impedance diagrams in both shape and size, in which a depressed semicircle at the high frequency part of the spectrum was observed and a second time constant appeared at low frequency region. The increase in size of the semicircle with inhibitor concentration means that the inhibitor effect increases as well.

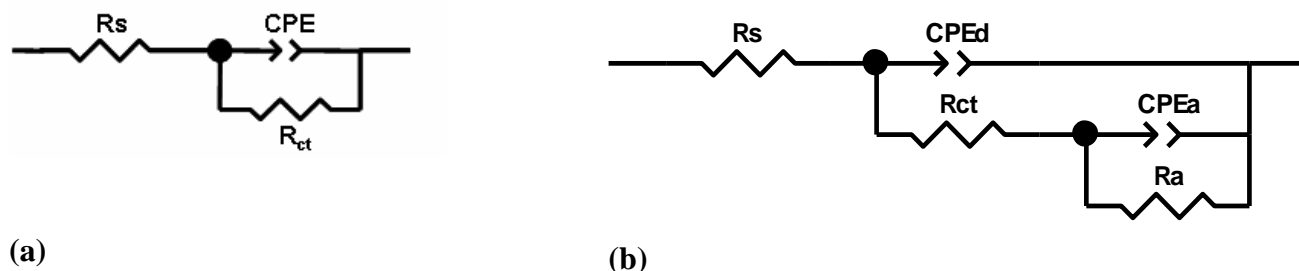


Figure 4. Electrical equivalent circuit used for modeling the interface carbon steel / 1 M HCl solution without and with 3-PYP.

The first capacitive loop (the larger) appearing at high frequency region can be attributed to the charge transfer, the second one (the smaller) at low frequencies can be related to the adsorption of inhibitor molecules on the metal surface and/or all other accumulated kinds at the metal/solution interface (inhibitor molecules, corrosion products, etc.) [76]. In this case, the structural model of Fig. 4a is inadequate (see Fig. 6, representative example) and a two-time-constant model should be used to describe the electrochemical impedance spectra in the presence of 3-PYP, as presented in Fig. 4b, that provides the determination of the adsorption parameters R_a and CPE_a (A_a and n_a , respectively). In Fig. 4b, R_s represent the solution resistance, R_{ct} is the charge transfer resistance and CPE_d represent the capacitance of the high frequency semicircle that can be attributed to the charge transfer process. R_a represents the resistance of the adsorbed inhibitor and CPE_a is the capacitance of the inhibitor film due to the inhibitor’s adsorption on the steel surface.

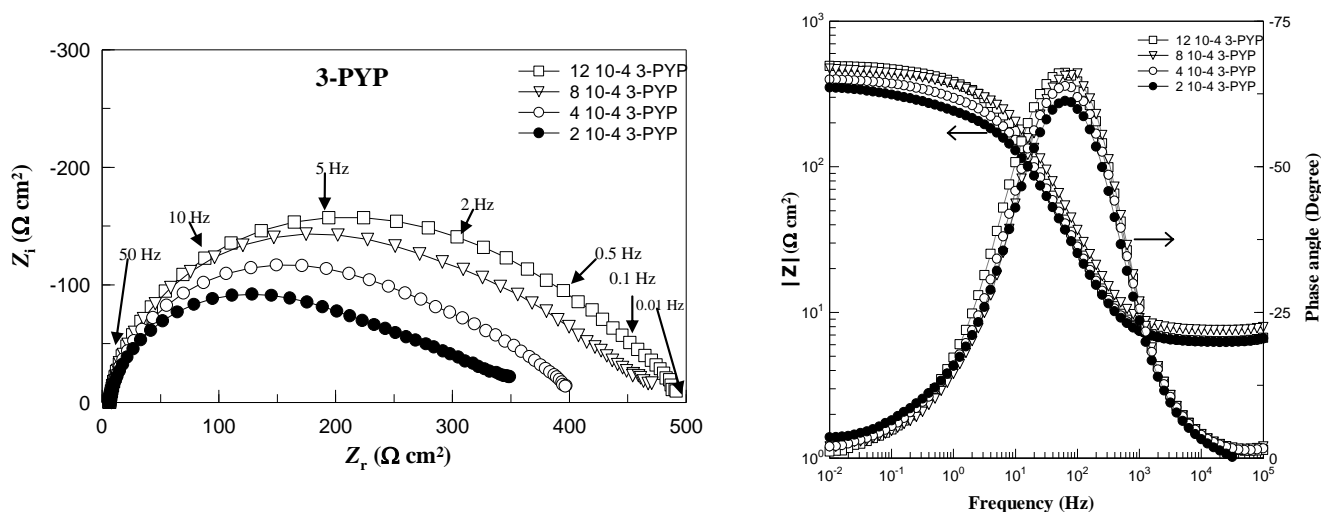


Figure 5. Nyquist and Bode diagrams for carbon steel in 1 M HCl containing different concentrations of 3-PYP after 24 h of immersion period at 30°C.

The time constant of the adsorption process is $\tau_a = C_a R_a$, the adsorption capacitance being again replaced by a CPE, and C_a is calculated using Eq. (6). The experimental data were very well fitted according to the proposed equivalent circuit and as an example; the calculated curves are presented in Fig. 7. This model is valid for all concentrations of 3-PYP and it is well representative of the phenomena which may occur in the investigated steel/3-PYP/HCl system, both in the HF and in the LF parts of the spectra. The main fitted parameters are summarised in Table 3.

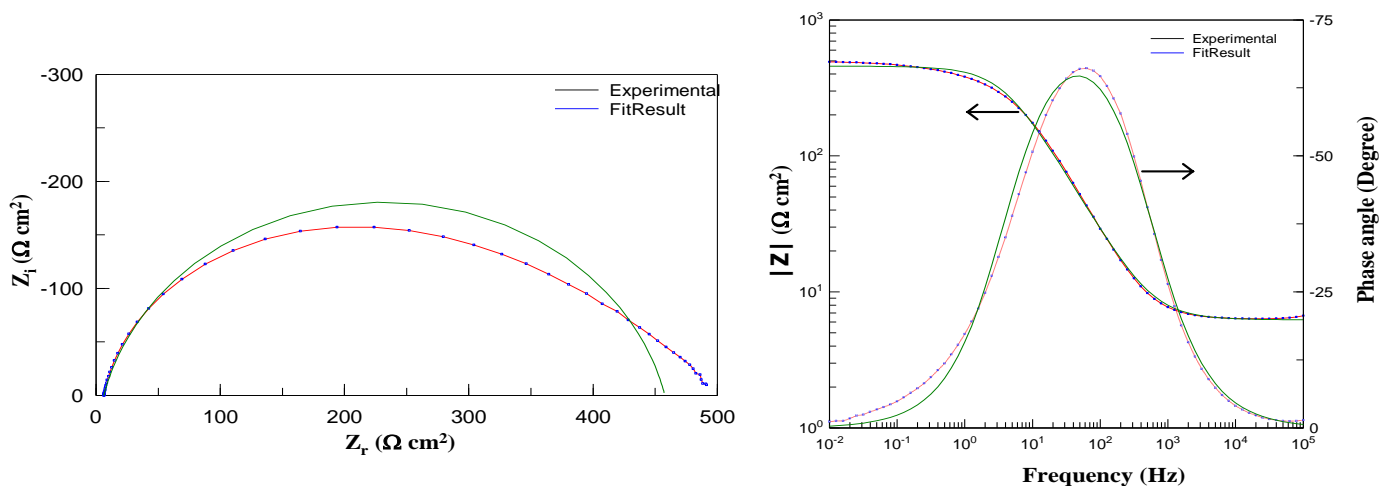


Figure 6. EIS Nyquist and Bode diagrams for carbon steel / 1 M HCl + 1.2 mM of 3-PYP interface: (···) experimental; (—) fitted data using structural model in Fig. 4a.

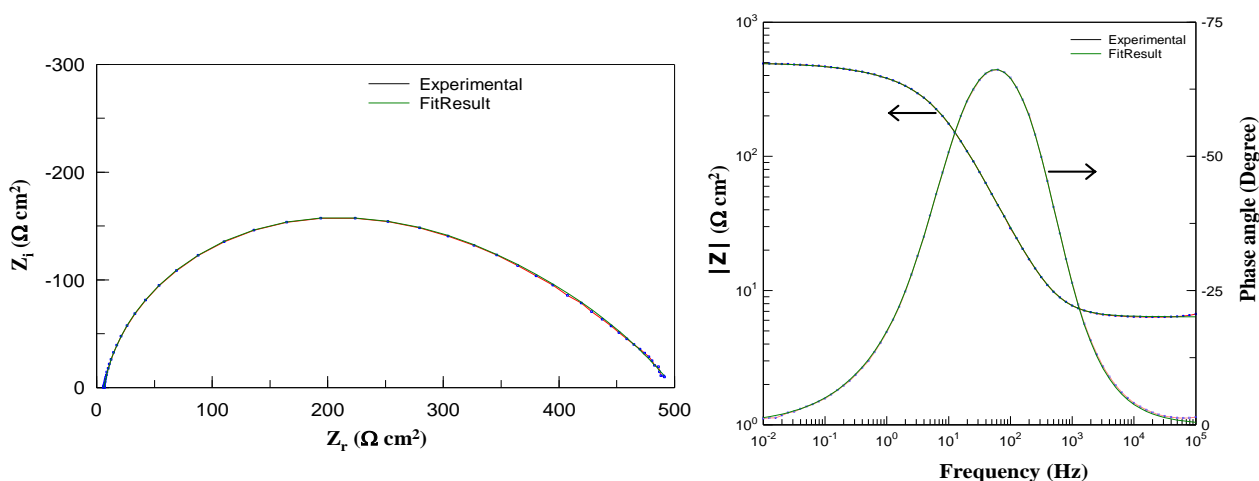


Figure 7. EIS Nyquist and Bode diagrams for carbon steel / 1 M HCl + 1.2 mM of 3-PYP interface: (···) experimental; (—) fitted data using structural model in Fig. 4b.

Estimates of the margins of error calculated for the parameters are also presented in this Table. The data are found to be sufficiently well fitted within the limits of experimental error and reproducibility of data. Inspection of the fitting results (Table 3), shows clearly that R_{ct} and C_{dl} values have opposite trend at the whole concentration range (R_{ct} increases and C_{dl} decreases with inhibitor concentration). A large R_{ct} is associated with a slower corroding system [71,77]. Furthermore, the

decrease in the C_{dl} with increase in 3-PYP concentrations may be attributed to the formation of a protective layer on the carbon steel surface [78]. The increase of the n_d value after addition of 3-PYP in the corrosive solution can corroborate this assumption. Indeed, the value of n_d grows as well (0.891-0.927), when compared to that obtained in pure 1 M HCl (0.879). This can be attributed to a certain decrease in the initial surface in homogeneity resulting from the adsorption of 3,6-bis(3-pyridyl)pyridazine molecules on the most active adsorption centres at the carbon steel surface [71]. Also, the addition of 3-PYP to the corrosive solution increases slightly the time constant (τ_d) value with opposite trend of C_{dl} (Table 3). For example, when the 3-PYP concentration is increased to 1.2 mM in the corrosive medium, the interface (τ_d) parameter increases from 0.0194 to 0.022 s while the C_{dl} value decreases from 524 to 70 $\mu\text{F cm}^{-2}$, signifying that the charge and discharge rates to the metal-solution interface is greatly decreased. This shows that there is agreement between the amount of charge that can be stored (i.e. capacitance) and the discharge velocity in the interface (τ_d) [79]. In the case of 3-PYP addition, the resistance R_a has small values compared to R_{ct} values (the total resistance R_p is dominated by R_{ct}) and increases significantly with 3-PYP concentration. However, the C_a values have opposite trend as that of R_a values at the whole concentration range, while practically no change is observed in the value of n_a . The values of n_a are lower than that of n_d , indicating greater energy distribution in the adsorption layer [75]. The time constants τ_a shows a marked tendency to decrease with concentration and its values are much higher than τ_d . As in the case of n_a the apparent decrease of τ_a with concentration is influenced by the adsorption process.

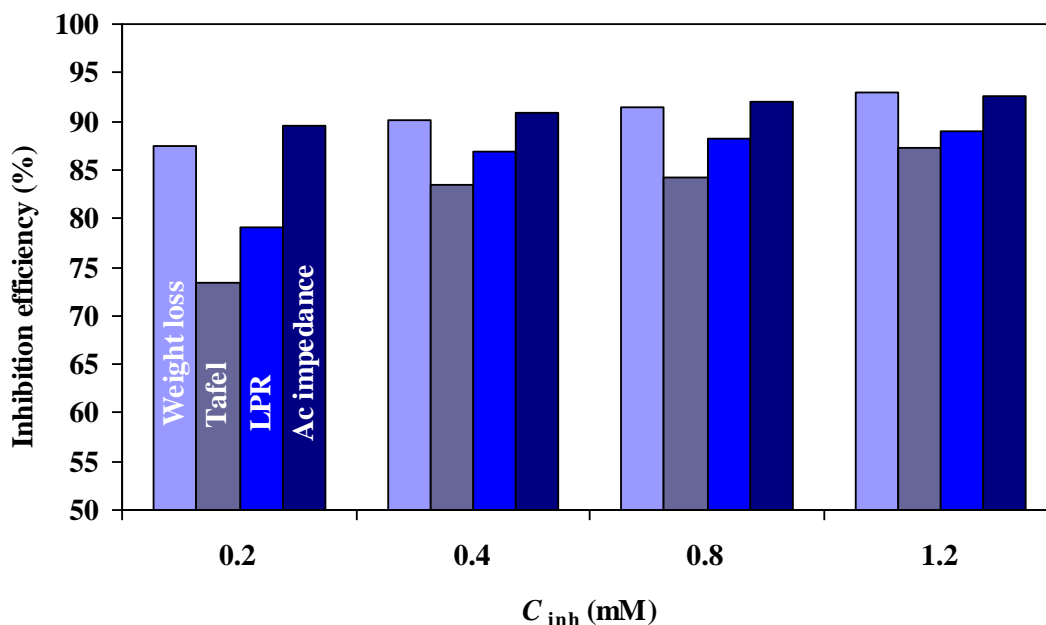


Figure 8. Variation of inhibition efficiency of 3-PYP with concentration.

In the absence of inhibitor molecules, the ac resistance polarisation, R_p , consists of only charge transfer resistance (R_{ct}), while in the presence of inhibitor, the sum of R_{ct} and R_a are equivalent to R_p . The related inhibition efficiency, $\eta_z(\%)$, is calculated from $R_p = (R_{ct} + R_a)$ using the following equation:

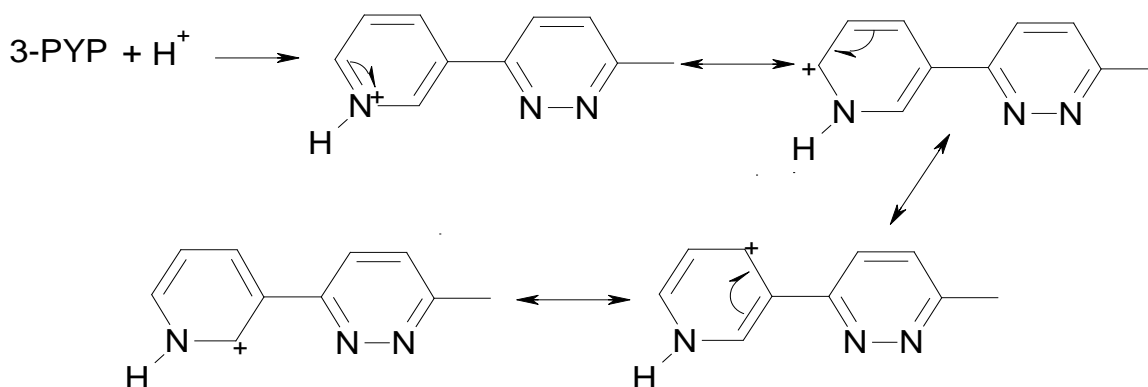
$$\eta_z(\%) = \frac{R_{p(i)} - R_p}{R_{p(i)}} \times 100 \quad (8)$$

where R_p and $R_{p(i)}$ are the ac polarisation resistance of carbon steel electrode in the uninhibited and inhibited solutions, respectively. It is obvious that the increase in inhibitor concentration enhances R_p , and consequently improves the inhibition efficiency till reaching their maximum value at 1.2 mM ($R_p = 493.4 \Omega \text{ cm}^2$, $\eta_z(\%) = 92.5$). The $\eta(\%)$ values obtained from the ac impedance technique are comparable and run parallel with those obtained from the weight loss measurements, the potentiodynamic and the LPR methods (Fig. 8).

3.2. Adsorption isotherm and surface analysis

Corrosion inhibition of carbon steel in 1 M HCl solution by 3,6-bis(3-pyridyl)pyridazine (3-PYP) can be explained by molecular adsorption. Two main types of interaction can describe the adsorption of the organic compound: physical adsorption and chemisorption. There are influenced by the chemical structure of the organic compounds, the distribution of charge in the molecule, the nature and surface charge of the metal and the type of aggressive media [44].

In aqueous hydrochloric acid medium, the 3-PYP can be protonated at the N heteroatom in the pyridinium cycle, with respect to the pK_a of the protonated function, as shown in the following scheme:



Owing to the acidity of the medium, 3-PYP derivative can exist as neutral species or in cationic forms (3-PYPH^+). Thus, 3-PYP molecules may be adsorbed on the metal surface in different ways: (i) it was reported that the surface charge of steel at E_{corr} in 1 M HCl solution is expected to be positive [80]. Accordingly, the adsorption of the cationic 3-PYP species does not take place. Instead, the adsorption of Cl^- anions occurs and the surface becomes negatively charged. Due to the electrostatic attraction, the cationic forms of inhibitor (3-PYPH^+) are adsorbed through electrostatic interactions (physical adsorption) between positively charged nitrogen atoms in the pyridinium cycle and negatively charged carbon steel surface [42]; (ii) the adsorption of the 3-PYP molecules can occur due

to the formation of links between the d-orbital of iron atoms (chemisorption), involving the displacement of water molecules from the metal surface, by the lone sp^2 electron pairs present on the N atoms of both the heterocyclic rings (pyridinium and pyridazyl) and/or the π electrons of heterocyclic rings [81], (iii) the adsorption mechanism of 3-PYP on carbon steel surface involves both types of interactions, physisorption (ionic) and chemisorption (molecular).

In order to rationalize and to get more information, the experimental data have been tested with several adsorption isotherms that provide information about the interaction among the adsorbed molecules themselves and their interactions with the electrode surface. Several adsorption isotherms (Langmuir, Temkin, Frumkin,...) were assessed and the Temkin adsorption isotherm was found to provide the best description of the adsorption behaviour of the investigated pyridazine (Fig. 9). The Temkin isotherm is given by the following equation [82]:

$$\theta = \frac{1}{f} \ln(K_{\text{ads}} C_{\text{inh}}) \quad (9)$$

where θ is the fractional surface coverage; f is the molecular interaction constant; C_{inh} is the inhibitor concentration; and K_{ads} is the equilibrium constant of the adsorption process. The fractional surface coverage θ can be easily determined from ac impedance or the weight loss measurements by the ratio $\eta(\%) / 100$, if one assumes that the values of $\eta(\%)$ do not differ substantially from θ (the impedance and gravimetric data are collected in a time interval of 24 h, considered sufficient for adsorption equilibrium to be achieved) [1,80].

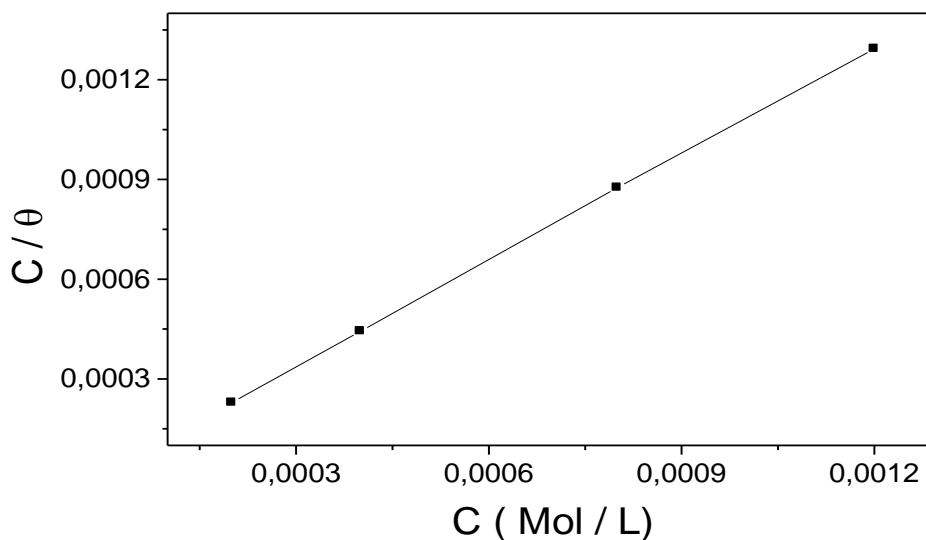


Figure 9. Temkin adsorption plot for carbon steel in 1 M HCl containing 3-PYP at 30°C.

The plot of θ versus $\log C_{\text{inh}}$, in Fig. 9, yields straight line with the regression coefficient (R^2) very closed to 1.00, clearly proving that the adsorption of 3-PYP on the carbon steel obeys the Temkin

adsorption isotherm which is characteristic of a multi-layer adsorption (interaction between the adsorbed species). This behaviour can be explained by the fact that the 3-PYP molecule possesses several favorable factors for strong adsorption such as the presence of four nitrogen atoms, three aromatic rings and an ideal plane structure, that can make the electronic effects more important and the steric effects omitted [83]. In this way, we have used DFT method in order to understand the structural effect on the corrosion inhibition properties of 3-PYP. Two conformations were calculated for non protonated or protonated N heteroatom in the pyridinium cycle. Effectively, the 3,6-bis(3-pyridyl)pyridazine (3-PYP) can be protonated in 1 M HCl solution at N heteroatom in the pyridinium cycle due to its pK_a value of 4.3. The optimized structures in the solvent are given in Fig. 10.

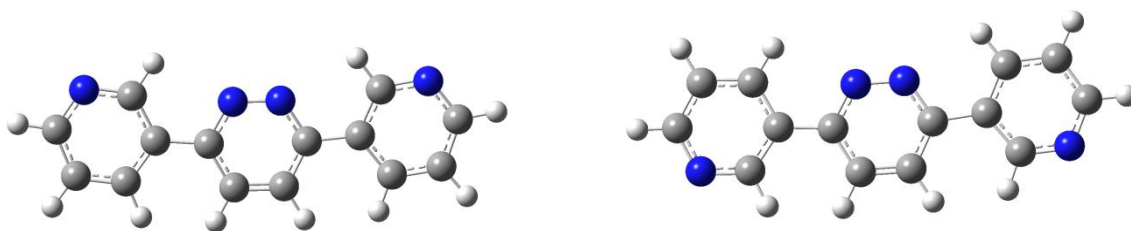


Figure 10. Optimized molecular structures of 3-PYP in solvent.

The difference energy between these two cis/trans conformations is about $-0.5 \text{ kcal mol}^{-1}$ for the trans one in the solvent assuming that these two conformations can be realistic. The two calculated conformations are full plane, no distortion between pyridinium and pyridazine cycles can be observed. This structural result can corroborate the multi-layer adsorption of 3-PYP on the steel surface (Temkin model). In order to explain this behaviour, the electronic properties of 3-PYP is inspected. It's well known that the reactive ability of the inhibitor is considered to be closely related to their frontier molecular orbitals. A typical electron density distribution of the highest occupied molecular orbital (HOMO) for diprotonated 3-PYP (3-PYPH_2^{2+}) are shown in Fig. 11.



Figure 11. The frontier molecular orbital density distributions (HOMO) along the more energetically stable conformations of diprotonated 3-PYP.

The HOMO density is mainly localized on the two nitrogen of the pyridazine ring that can confer the electron donation properties and can induce the adsorption of the 3-PYP molecules on the steel surface with stabilization by intermolecular hydrogen bonding between pyridinium rings (Fig.

12). In the solid state, extensive π - π stacking between the aromatic systems can be observed in the case of pyridylpyridazines [84]. It has been shown that electron-poor aromatic rings interact with electron-rich aromatic groups [85,86]. Hence, it can be suggested that, after the adsorption of 3-PYP cationic species on the steel surface, the electron-poor group (pyridazine ring) interacts with the less electron-poor ring (pyridinium ring). Indeed, the protonated 3-PYP species can be assembled into stacks (Fig. 13A), where each molecule has two offset π -stacked interactions with each neighbouring molecule [86]. Such an arrangement allows for neighbouring molecules within a stack to have two π - π interactions, between relatively electron-rich (pyridinium) and electron-poor (pyridazine) rings. Also, it is possible to imagine a structure in which the three aromatic rings participate in π - π interactions (Fig. 13B). However, in such a case, π - π interactions act between identical rings and this is less favourable than the first proposed arrangement [86].

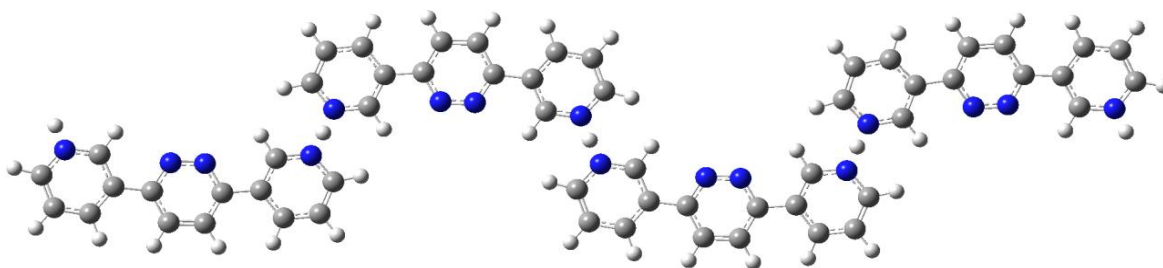


Figure 12. 3-PYP molecules stabilized by intermolecular hydrogen bonding.

From the slope and the intercept of the straight line (Fig. 9), the adsorption parameters values can be calculated; $f = 57.8$ and $K_{\text{ads}} = 1.46 \cdot 10^{26} \text{ M}^{-1}$. K_{ads} is related to the standard Gibbs free energy of adsorption, $\Delta G^{\circ}_{\text{ads}}$, according to [20]:

$$K_{\text{ads}} = \frac{1}{55.55} \exp\left(\frac{-\Delta G^{\circ}_{\text{ads}}}{RT}\right) \quad (10)$$

where R is the universal gas constant and T is the absolute temperature. The value 55.55 in the above equation is the concentration of water in solution in mol/l. The calculated $\Delta G^{\circ}_{\text{ads}}$ value is $-161.88 \text{ kJ mol}^{-1}$. The negative values of $\Delta G^{\circ}_{\text{ads}}$ ensure the spontaneity of the adsorption process and the stability of the adsorbed layer on the steel surface. It's well known that the adsorption type is regarded as physisorption if the absolute value of $\Delta G^{\circ}_{\text{ads}}$ was of the order of 20 kJ mol^{-1} or lower. The inhibition behaviour is attributed to the electrostatic interaction between the organic molecules and iron atom. When the absolute value of $\Delta G^{\circ}_{\text{ads}}$ is of the order of 40 kJ mol^{-1} or higher, the adsorption could be seen as chemisorption. In this process, the covalent bond is formed by the charge sharing or transferring from the inhibitor molecules to the metal surface [67]. The calculated $\Delta G^{\circ}_{\text{ads}}$ value in this work ($-161.88 \text{ kJ mol}^{-1}$) indicates, therefore, that the adsorption mechanism of 3-PYP on carbon steel in 1 M HCl solution is mainly due to chemisorption. Moreover, the large negative value of $\Delta G^{\circ}_{\text{ads}}$ suggests that this inhibitor is strongly adsorbed on the steel surface [30]. This conclusion is in agreement with

the findings of other workers [30,80]. In addition, it was reported that the constant f is related to the molecular interactions in the adsorption layer as well as energetic inhomogeneity of the surface [87]. If f is positive, mutual attraction of molecules occurs and if f is negative repulsion takes place. The positive and high value of the molecular interaction constant ($f = 57.8$) indicates the existence of a strong attractive interaction between adsorbed 3-PYP molecules in the adsorbed layer and this results in strong adsorption.

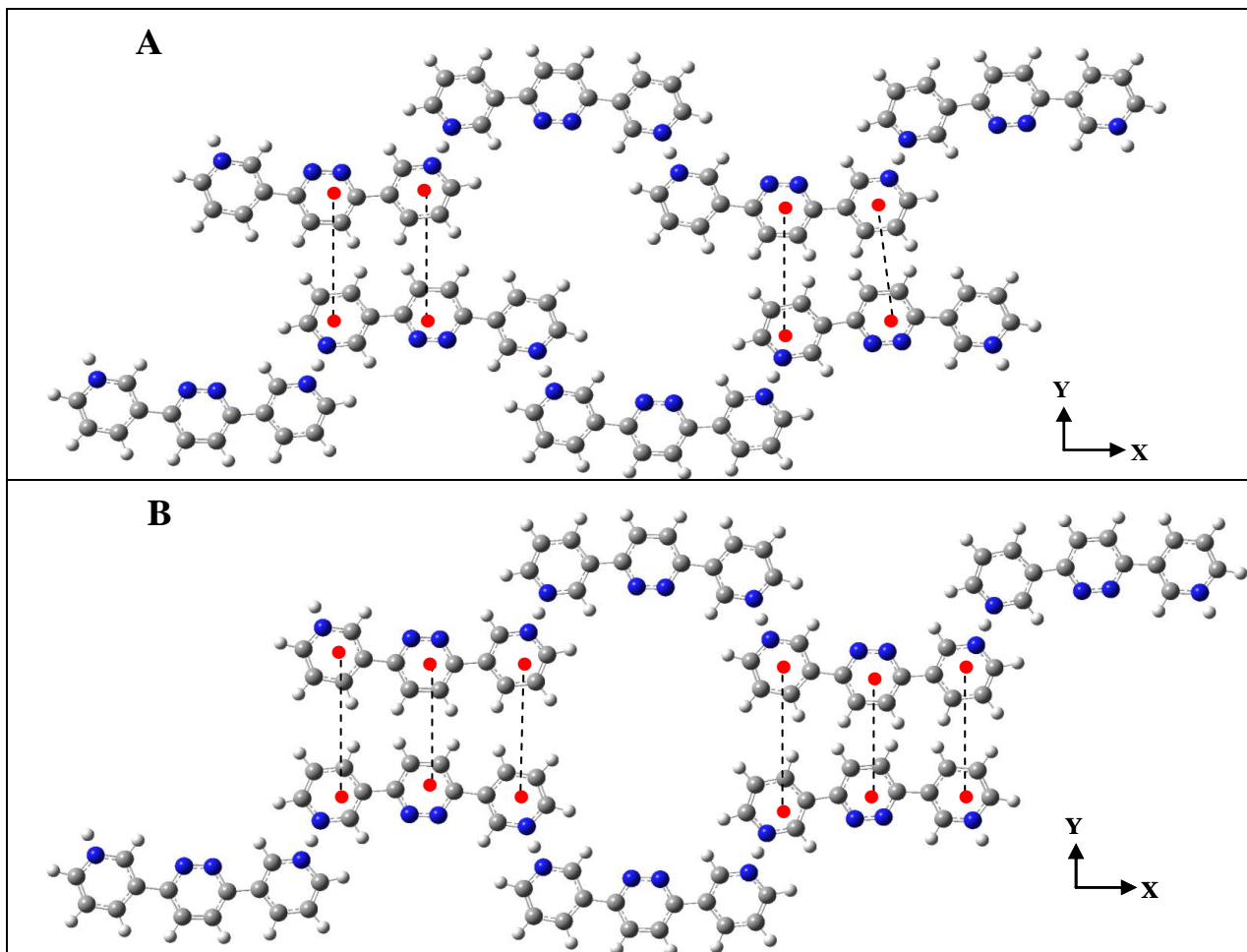


Figure 13. π - π Stacking models of 3-PYP molecules (the centroids of aromatic rings are shown as red circles).

In order to confirm this assumption (chemisorption) and elucidate the nature of the organic thin film formed on the steel surface, the surface analysis (XPS) study are given and discussed below. XPS technique was used to investigate the composition of the organic adsorbed layer on the carbon steel surface in normal hydrochloric medium by 3-PYP. In this way, the spectra (C 1s and N 1s) for pure 3-PYP are presented in Fig. 14 and the high-resolution peaks for C 1s, N 1s, O 1s and Fe 2p for carbon steel surface after 24 h of immersion in 1 M HCl solution containing 1.2 mM of 3,6-bis(3-pyridyl)pyridazine (3-PYP), are also recorded and given in Fig. 15, respectively (at this concentration, the highest inhibition efficiencies were achieved as previously shown). All XPS spectra contained complex forms, which were assigned to the corresponding species through a deconvolution fitting

procedure (a non-linear least squares algorithm with a Shirley base line and a Gaussian–Lorentzian combination) using the XPS Peak-Fit 4.1 software. The obtained values of binding energy (BE) are summarised in Table 4. The values in bracket represent the relative percentage of the peak component. The XPS results for untreated carbon steel are also presented in Table 4 in order to facilitate comparison [88].

The deconvoluted C 1s spectrum for pure 3-PYP shows two main peaks (Fig. 14, Table 4). The first peak located at approx. 285.0 eV has the largest contribution and is attributed to the C–C, C=C and C–H aromatic bonds [30]. The second peak at 286.3 eV is attributed to the C–N and C=N bonds in the pyridinium and the pyridazine rings [30]. After acidic immersion, the deconvoluted C 1s spectrum for 3-PYP-treated carbon steel shows three main peaks (Fig. 15, Table 4). Indeed, the first component at a BE ~ 285.0 eV, which is the largest contribution, is attributed to the C–C, C=C and C–H aromatic bonds; the second component may be assigned to the carbon atoms bonded to nitrogen in C–N and C=N bonds in the pyridazine and the pyridinium rings at 286.5 eV; the last component at higher binding energy (located at approx. 288.7 eV) may be ascribed to the carbon atom of the C=N⁺ [89].

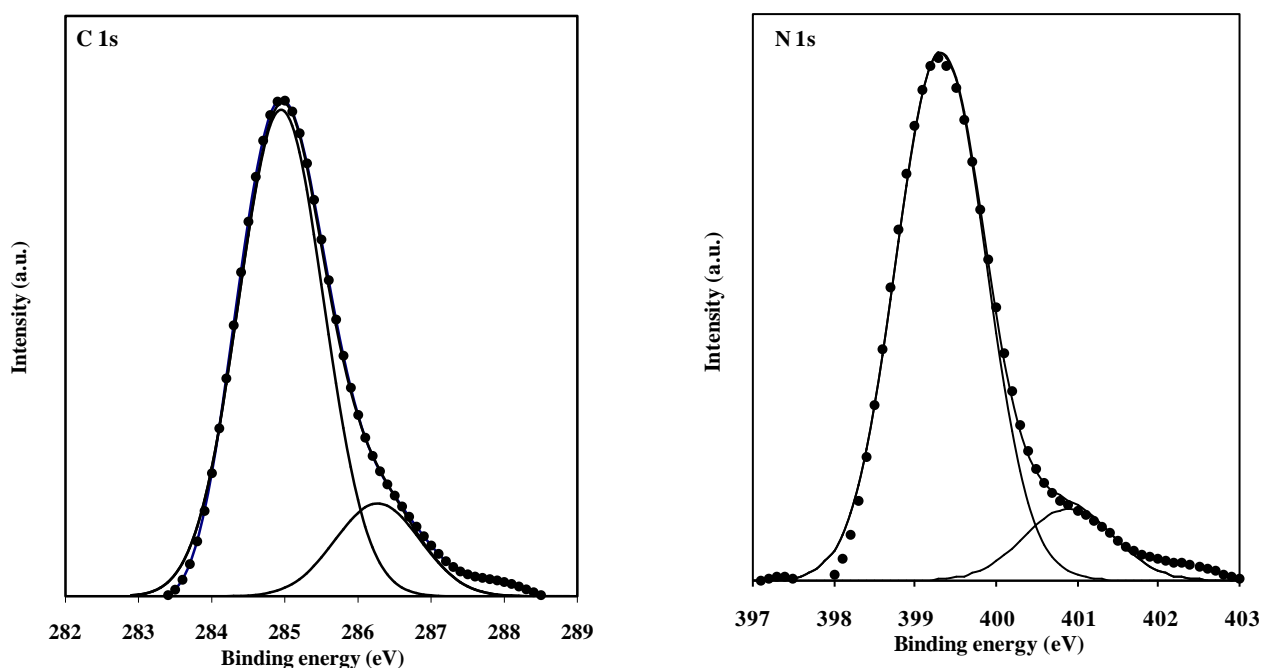


Figure 14. The XPS deconvoluted profiles of C 1s and N 1s for pure 3-PYP.

The N 1s XPS spectrum for 3-PYP-treated carbon steel is fitted into two components (Fig. 15), located around at 400.0 and 401.8 eV. The first component has the largest contribution and is mainly attributed to the unprotonated N atom (=N– structure) in the pyridinium and the pyridazine rings [38]. In comparison with N 1s spectrum of pure 3-PYP (Fig. 14), the peak of =N– structure is expected to appear at somewhat higher position than the one observed (399.3 eV) in pure 3-PYP because the coordination to the steel surface caused the peak shift toward higher binding energy [90]. From these

previous observations, our XPS results are consistent with the thermodynamic assumption that the 3-PYP was chemisorbed on the steel surface. The second component is attributable to the oxidized nitrogen as a result of the protonation of the nitrogen in the pyridazine ring ($=N^+H^-$), which due to the increase of the positive charge on the nitrogen atom, a core-level chemical shift to higher binding energy is produced [91,92].

Table 4. Binding energies (eV), relative intensity and their assignment for the major core lines observed for untreated carbon steel, pure 3-PYP and 3-PYP-treated carbon steel substrate.

Substrate	C 1s		O 1s		N 1s		Fe 2p		
	BE / eV	Assignment	BE / eV	Assignment	BE / eV	Assignment	BE / eV	Assignment	
Carbon steel before immersion [88]			529.9 (45 %)	Fe ₂ O ₃ /Fe ₃ O ₄	—	—	706.1 (46 %)	Fe ⁰	
			531.2 (37 %)	FeOOH/Fe(OH) ₃	—	—	710.5 (9 %)	Fe ₂ O ₃ / Fe ₃ O ₄ /FeOOH	
			532.8 (18 %)	Adsorbed H ₂ O	—	—	714.9 (13 %)	Satellite of Fe(II)	
					—	—	719.6 (24%)	Satellite of Fe(III)	
						—	—	724.4 (8 %)	Fe 2p _{1/2}
Pure 3-PYP	285.0 (84 %)	C–C/C=C/C–H	—	—	399.3 (88 %)	=N–N/N=C	—	—	
	286.3 (16 %)	C–N/C=N	—	—	400.9 (12 %)	Oxidized nitrogen	—	—	
3-PYP/Carbon steel after immersion	285.0 (50 %)	C–C/C=C/C–H	530.2 (40 %)	Fe ₂ O ₃ /Fe ₃ O ₄	400.0 (85 %)	=N–N/N=C	707.1 (6 %)	Fe ⁰	
	286.5 (17 %)	C–N/C=N	531.8 (47 %)	FeOOH/Fe(OH) ₃	401.8 (81 %)	=N ⁺ H ⁻	711.0 (44 %)	Fe ₂ O ₃ / Fe ₃ O ₄ /FeOOH	
	288.7 (33 %)	C=N ⁺	532.9 (13 %)	Adsorbed H ₂ O	—	—	713.7 (19 %)	FeCl ₃	
					—	—	719.5 (10 %)	Satellite of Fe(III)	
						—	—	724.4 (21 %)	Fe 2p _{1/2}

The deconvolution of the O 1s spectrum for carbon steel surface after immersion in 1 M HCl solution containing 3-PYP may be fitted into three main peaks (Fig. 15). The first peak (located at approx. 530.2 eV) is attributed to O²⁻, and in principle could be related to oxygen atoms bonded to Fe³⁺ in the FeO and/or Fe₂O₃ oxides [93]. The second peak (located at approx. 531.8 eV) is ascribed to OH⁻, is attributable to oxygen in hydrous iron oxides, such as FeOOH and/ or Fe(OH)₃ [93]. Finally, the third peak at 532.9 eV may be assigned to oxygen of adsorbed water [94].

The Fe 2p spectrum for 3PYP-treated steel surface was fitted using two doublets, 711 eV (Fe 2p_{3/2}) and 724.1 eV (Fe 2p_{1/2}), with an associated ghost structure (Fig. 15 and Table 4). The deconvolution of the high resolution Fe 2p_{3/2} XPS spectrum consists in four peaks. These peaks may be assigned as being due to iron in environments associated with iron oxide and hydroxide. Indeed, the first peak located at 707.1 was assigned to metallic iron (Fe⁰) [92,95]. The second peak at a BE ~ 711.0 eV assigned to Fe³⁺ as mentioned in [90], was attributed to ferric compounds such as Fe₂O₃ (i.e., Fe³⁺ oxide) and/or Fe₃O₄ (i.e., Fe²⁺/Fe³⁺ mixed oxide) and FeOOH (i.e., oxyhydroxyde), [96,97], while that located at around 713.7 eV is attributed to the presence of a small concentration of FeCl₃ on the metal surface [98,99].

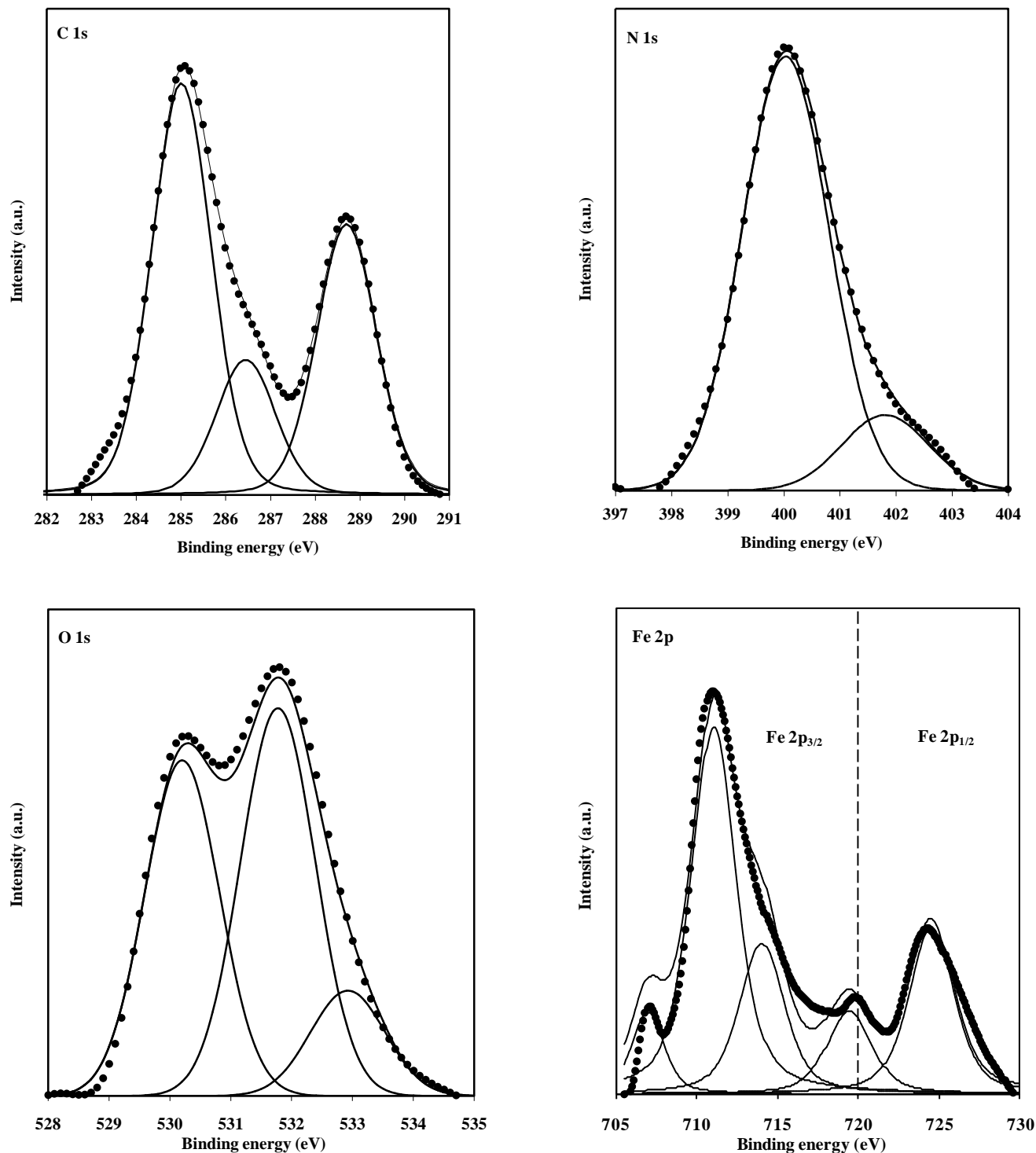


Figure 15. The XPS deconvoluted profiles of C 1s, O 1s, N 1s and Fe 2p for carbon steel after 24 h immersion period in 1 M HCl in the presence of 1.2 mM of 3-PYP at 30 °C.

The last peak, observed at 719.5 eV is ascribed to the satellites of the ferric compounds as mentioned previously [95]. Inspection of the Fe 2p_{3/2} XPS results for 3-PYP-treated carbon steel after immersion in HCl medium shows that in comparison with untreated surface steel (Table 4) the

aggressive solution induced an imbalance in favor of Fe^{3+} in the proportion $\text{Fe}^{3+}/\text{Fe}^0$: the component centred at 711.0 eV becomes prevalent (Table 4). The significant decrease in Fe^0 amount established therefore that the steel surface becomes largely oxidised in acid solution.

On the basis of XPS analyses, the obtained results give evidence of chemical interactions between the 3-PYP inhibitor and carbon steel surface. Indeed, the presence of nitrogen species on the steel surface, such as $=\text{N}-$ structure and $\text{N}-\text{C}$, confirms that the investigated pyridazine was chemisorbed on the carbon steel surface and corroborates the thermodynamic study. Thus 3-PYP can be regarded as good inhibitor for carbon steel corrosion in normal hydrochloric acid medium.

4. CONCLUSION

Concluding the experimental part, it was clearly demonstrated that all techniques used, especially electrochemical techniques, are able to characterize and to follow the corrosion inhibition process promoted by 3,6-bis(3-pyridyl)pyridazine (3-PYP). It was shown that 3-PYP exhibits good inhibition properties for the corrosion of carbon steel in 1 M HCl solutions at 30°C, and the corrosion inhibition efficiency increases with increasing the inhibitor concentration. The corrosion inhibition efficiencies, determined by weight loss, polarisation and EIS methods are in reasonable agreement. The polarisation curves indicate a mixed-type suppression of both anodic and cathodic processes. In the presence of 3-PYP, the impedance spectra are well described by a structural model of the interface carbon steel/1 M HCl + inhibitor with two time constants – they are attributed to the double layer charging and adsorption of the inhibitor. Both double-layer and adsorption capacitances are distributed and therefore modelled by constant phase elements (CPE) due to the surface inhomogeneity. The adsorption of 3-PYP obeys the Temkin adsorption isotherm. The thermodynamic parameters and XPS analysis reveal that the inhibition of corrosion by 3-PYP is due to the formation of a chemisorbed film on the metal surface.

ACKNOWLEDGEMENTS

Prof S. S. Al-Deyab and Prof B. Hammouti extend their appreciation to the Deanship of Scientific Research at King Saud University for funding the work through the research group project.

References

1. F. Bentiss, M. Bouanis, B. Mernari, M. Traisnel, H. Vezin, M. Lagrenée, *Appl. Surf. Sci.* 253 (2007) 3696–3704 (and references therein).
2. M.A. Amin, S.S. Abd El-Rehim, E.E.F. El-Sherbini, R.S. Bayyomi, *Electrochim. Acta* 52 (2007) 3588.
3. P. Bommersbach, C. Alemany-Dumont, J.P. Millet, B. Normand, *Electrochim. Acta* 51 (2005) 1076–1084.
4. M.A. Quraishi, J. Rawat, *Mater. Chem. Phys.* 77 (2002) 43–47.
5. M. Lagrenée, B. Mernari, M. Bouanis, M. Taisnel, F. Bentiss, *Corros. Sci.* 44 (2002) 573–588.

6. I. El Ouali, B. Hammouti, A. Aouniti, Y. Ramli, M. Azougagh, E.M. Essassi, M. Bouachrine, *J. Mater. Environ. Sci.* 1 (2010) 1–8.
7. F. Bentiss, M. Traisnel, L. Gengembre, M. Lagrenée, *Appl. Surf. Sci.* 161 (2000) 194–202.
8. E.M. Sherif, S.-M. Park, *Electrochim. Acta* 51 (2006) 1313–1321.
9. S.L. Granese, B.M. Rosales, C. Oviedo, J.O. Zerbino, *Corros. Sci.* 33 (1992) 1439–1453.
10. F. Bentiss, M. Bouanis, B. Mernari, M. Taisnel, M. Lagrenée, *J. Appl. Electrochem.* 32 (2002) 671–672.
11. F. Bentiss, M. Lagrenée, M. Traisnel, J.C. Hornez, *Corros. Sci.* 41 (1999) 789–803.
12. F. Bentiss, M. Lagrenée, M. Traisnel, B. Mernari, H. Elattari, *J. Appl. Electrochem.* 29 (1999) 1073–1078.
13. F. Bentiss, M. Traisnel, H. Vezin, M. Lagrenée, *Indus. Eng. Chem. Res.* 39 (2000) 3732–3736.
14. F. Bentiss, M. Traisnel, M. Lagrenée, *Brit. Corros. J.* 35 (2000) 315–320.
15. B. El Mehdi, B. Mernari, M. Traisnel, F. Bentiss, M. Lagrenée, *Mater. Chem. Phys.* 77 (2003) 489–496.
16. L. Wang, *Corros. Sci.* 48 (2006) 608–616.
17. H.-L. Wang, H.-B. Fan, J.-S. Zheng, *Mater. Chem. Phys.* 77 (2003) 655–661.
18. M.A. Quraishi, H.K. Sharma, *Mater. Chem. Phys.* 78 (2003) 18–21.
19. M. Lebrini, M. Traisnel, M. Lagrenée, B. Mernari, F. Bentiss, *Corros. Sci.* 50 (2008) 473–479.
20. F. Bentiss, C. Jama, B. Mernari, H. El Attari, L. El Kadi, M. Lebrini, M. Traisnel, M. Lagrenée, *Corros. Sci.* 51 (2009) 1628–1635.
21. F. Bentiss, M. Lagrenée, M. Traisnel, J.C. Hornez, *Corrosion* 55 (1999) 968–976.
22. M.A. Quraishi, D. Jamal, *Mater. Chem. Phys.* 71 (2001) 202–205.
23. F. Bentiss, M. Traisnel, M. Lagrenée, *Corrosion* 56 (2000) 733–742.
24. F. Bentiss, M. Traisnel, M. Lagrenée, *Corros. Sci.* 42 (2000) 127–146.
25. M. Lagrenée, B. Mernari, N. Chaibi, M. Traisnel, H. Vezin, F. Bentiss, *Corros. Sci.* 43 (2001) 951–953.
26. F. Bentiss, M. Traisnel, N. Chaibi, B. Mernari, H. Vezin, M. Lagrenée, *Corros. Sci.* 44 (2002) 2271–2289.
27. F. Bentiss, M. Traisnel, H. Vezin, H. F. Hildebrand, M. Lagrenée, *Corros. Sci.* 46 (2004) 2781–2792.
28. M. Lebrini, F. Bentiss, H. Vezin, M. Lagrenée, *Appl. Surf. Sci.* 252 (2005) 950–958.
29. M. Bouklah, B. Hammouti, M. Lagrenée, F. Bentiss, *Corros. Sci.* 48 (2006) 2831–2842.
30. M. Outirite, M. Lagrenée, M. Lebrini, M. Traisnel, C. Jama, H. Vezin, F. Bentiss, *Electrochim. Acta* 55 (2010) 1670–1681.
31. F. Bentiss, M. Traisnel, M. Lagrenée, *J. Appl. Electrochem.* 31 (2001) 41–48.
32. M. El Azhar, B. Mernari, M. Traisnel, F. Bentiss, M. Lagrenée, *Corros. Sci.* 43 (2001) 2229–2238.
33. M. El Azhar, M. Traisnel, B. Mernari, L. Gengembre, F. Bentiss, M. Lagrenée, *Appl. Surf. Sci.* 185 (2002) 197.
34. F. Bentiss, M. Lebrini, H. Vezin, M. Lagrenée, *Mater. Chem. Phys.* 87 (2004) 18–23.
35. F. Bentiss, M. Lebrini, M. Traisnel, M. Lagrenée, *J. Appl. Electrochem.* 39 (2009) 1399–1407.
36. F. Bentiss, M. Lebrini, M. Lagrenée, *Corros. Sci.* 47 (2005) 2915–2931.
37. M. Lebrini, F. Bentiss, H. Vezin, M. Lagrenée, *Corros. Sci.* 48 (2006) 1279–1291.
38. M. Lebrini, M. Lagrenée, M. Traisnel, L. Gengembre, H. Vezin, F. Bentiss, *Appl. Surf. Sci.* 253 (2007) 9267–9276.
39. F. Bentiss, M. Lebrini, M. Lagrenée, M. Traisnel, A. Elfarouk, H. Vezin, *Electrochim. Acta* 52 (2007) 6865.
40. M. Lebrini, M. Lagrenée, H. Vezin, M. Traisnel, F. Bentiss, *Corros. Sci.* 49 (2007) 2254–2269.
41. F. Bentiss, M. Lebrini, H. Vezin, F. Chai, M. Traisnel, M. Lagrenée, *Corros. Sci.* 51 (2009) 2165–2173.
42. F. Bentiss, B. Mernari, M. Traisnel, H. Vezin, M. Lagrenée, *Corros. Sci.* 53 (2011) 487–495.

43. L. Wang, *Corros. Sci.* 43 (2001) 2281–2289.
44. A. Popova, M. Christov, S. Raicheva, E. Sokolova, *Corros. Sci.* 46 (2004) 1333–1350.
45. K.F. Khaled, *Electrochim. Acta* 48 (2003) 2493–2503.
46. A. Ouchrif, M. Zegmout, B. Hammouti, S. El-Kadiri, A. Ramdani, *Appl. Surf. Sci.* 252 (2005) 339–344.
47. M. Abdallah, *Mater. Chem. Phys.* 82 (2003) 786–792.
48. A. Chetouani, B. Hammouti, T. Benhadda, M. Daoudi, *Appl. Surf. Sci.* 249 (2005) 375–385.
49. M. Elayyachy, M. Elkodadi, A. Aouniti, A. Ramdani, B. Hammouti, F. Malek, A. Elidrissi, *Mater. Chem. Phys.* 93 (2005) 281–285.
50. Y. Yan, W.H. Li, L.K. Cai, B.R. Hou, *Electrochim. Acta* 53 (2008) 5953–5960.
51. X.H. Li, S.D. Deng, H. Fu, T.H. Li, *Electrochim. Acta* 54 (2009) 4089–4098.
52. X.H. Li, S.D. Deng, H. Fu, G.N. Mu, *Corros. Sci.* 51 (2009) 620–634.
53. S.A. Abd El-Maksoud, *Appl. Surf. Sci.* 206 (2003) 129–136.
54. L.B. Tang, X.M. Li, Y.S. Si, G.N. Mu, G.H. Liu, *Mater. Chem. Phys.* 95 (2006) 29–38.
55. A. Chetouani, B. Hammouti, A. Aouniti, N. Benchat, T. Benhadda, *Prog. Org. Coat.* 45 (2002) 373–378.
56. Chetouani, A. Aouniti, B. Hammouti, N. Benchat, T. Benhadda, S. Kertit, *Corros. Sci.* 45 (2003) 1675.
57. M. Bouklah, N. Benchat, A. Aouniti, B. Hammouti, M. Benkaddour, M. Lagrenée, H. Vezin, F. Bentiss, *Prog. Org. Coat.* 51 (2004) 118–124.
58. M. Bouklah, N. Benchat, B. Hammouti, A. Aouniti, S. Kertit, *Mater. Lett.* 60 (2006) 1901–1905.
59. M. Bouklah, A. Attayibat, S. Kertit, A. Ramdani, B. Hammouti, *Appl. Surf. Sci.* 242 (2005) 399–406.
60. M. Kissi, M. Bouklah, B. Hammouti, M. Benkaddour, *Appl. Surf. Sci.* 252 (2006) 4190–4197.
61. F. Bentiss, F. Gassama, D. Barbry, L. Gengembre, H. Vezin, M. Lagrenée, M. Traisnel, *Appl. Surf. Sci.* 252 (2006) 2684–2691.
62. S. Deng, X. Li, H. Fu, *Corros. Sci.* 53 (2011) 822–828.
63. M. Takahashi, T. Yamaoka, *Heterocycl. Commun.* 3 (1997) 521–526.
64. I. Ahamad, R. Prasad, M.A. Quraishi, *Corros. Sci.* 52 (2010) 933–942.
65. H.H. Hassan, E. Abdelghani, M.A. Amin, *Electrochim. Acta* 52 (2007) 6359–6366.
66. A.A. Aksüt, W.J. Lorenz, F. Mansfeld, *Corros. Sci.* 22 (1982) 611–619.
67. I. Ahamad, R. Prasad, M.A. Quraishi, *Corros. Sci.* 52 (2010) 1472–1481.
68. S.S. Abdel-Rehim, M.A.M. Ibrahim, K.F. Khaled, *Mater. Chem. Phys.* 70 (2001) 268–273.
69. J.O'M. Bockris, S. Srinivasan, *Electrochim. Acta* 9 (1964) 31–44.
70. A. Popova, E. Sokolova, S. Raicheva, M. Christov, *Corros. Sci.* 45 (2003) 33–58.
71. F.B. Growcock, J.H. Jasinski, *J. Electrochem. Soc.* 136 (1989) 2310–2314.
72. J.R. Macdonald, W.B. Johanson, in: J.R. Macdonald (Ed.), *Theory in impedance spectroscopy*, John Wiley & Sons, New York, 1987.
73. D.A. Lopez, S.N. Simison, S.R. de Sanchez, *Electrochim. Acta* 48 (2003) 845–854.
74. Z.B. Stoyanov, B.M. Grafov, B. Savova-Stoyanova, V.V. Elkin, *Electrochemical Impedance*, Nauka, Moscow, 1991.
75. A. Popova, M. Christov, A. Vasilev, *Corros. Sci.* 49 (2007) 3290–3302.
76. R. Solmaz, G. Kardaş, M. Çulha, B. Yazıcı, M. Erbil, *Electrochim. Acta* 53 (2010) 5941–5952.
77. M. Lebrini, F. Bentiss, N. Chihib, C. Jama, J.P. Hornez, M. Lagrenée, *Corros. Sci.* 50 (2008) 2914–2918.
78. M. Kedam, O.R. Mattos, H. Takenouti, *J. Electrochem. Soc.* 128 (1981) 266–274.
79. J. Morales Roque, T. Pandiyani, J. Cruz, E. García-Ochoa, *Corros. Sci.* 50 (2008) 614–624.
80. M.S. Morad, *Corros. Sci.* 50 (2008) 436–448.
81. M.M. El-Naggar, *Corros. Sci.* 49 (2007) 2226–2236.
82. W. Durnie, R.D. Marco, A. Jefferson, B. Kinsella, *J. Electrochem. Soc.* 146 (1999) 1751–1756.

83. J.H. Henríquez-Román, L. Padilla-Campos, M.A. Páez, J.H. Zagal, M.A. Rubio, C.M. Rangel, J. Costamagna, G. Cárdenas-Jirón, *J. Mol. Struct.: THEOCHEM* 757 (2005) 1–7.
84. F. Thébault, A.J. Blake, C. Wilson, N.R. Champness, M. Shröder, *New J. Chem.* 30 (2006) 1498–1508.
85. C.A. Hunter, J.K.M. Sanders, *J. Am. Chem. Soc.* 112 (1990) 5525–5534.
86. N.S. Oxtoby, A.J. Blake, N.R. Champness, C. Wilson, *CrystEngComm* 5 (2003) 82–86.
87. A.E. Stoyanova, E.I. Sokolova, S.N. Raicheva, *Corros. Sci.* 39 (1997) 1595–1604.
88. F.Z. Bouanis, F. Bentiss, S. Bellayer, M. Traisnel, J.B. Vogt, C. Jama, *Mater. Chem. Phys.* 127 (2011) 329.
89. J.F. Watts, J. Wolstenholme, *An introduction to surface analysis by XPS and AES*, John Wiley and Sons Inc., UK, 2003.
90. N. Nakayamaand, A. Obuchi, *Corros. Sci.* 45 (2003) 2075–2092.
91. G.A. Schick, Z. Sun, *Langmuir* 10 (1994) 3105–3110.
92. R. Devaux, D. Vouagner, A.M. De Becdelievre, C. Duret-Thual, *Corros. Sci.* 36 (1994) 171–186.
93. W. Temesghen, P.M.A. Sherwood, *Anal. Bioanal. Chem.* 373 (2002) 601–608.
94. K. Babić-Samardžija, C. Lupu, N. Hackerman, A.R. Barron, A. Luttge, *Langmuir* 21 (2005) 12187–12196.
95. V. Di castro, S. Ciampi, *Surf. Sci.* 331 (1995) 294–299.
96. M.A. Pech-Canul, P. Bartolo-Perez, *Surf. Coat. Technol.* 184 (2004) 133–140.
97. F.Z. Bouanis, F. Bentiss, M. Traisnel, C. Jama, *Electrochim. Acta* 54 (2009) 2371–2378.
98. V.S. Sastri, M. Elboujdaini, J.R. Romn, J.R. Perumareddi, *Corrosion* 52 (1996) 447–452.
99. F. Moulder, W.F. Stickle, P.E. Sobol, K.D. Bomben, in: J. Chastain (Ed.), *Handbook of X-Ray Photoelectron Spectroscopy*, Perkin-Elmer Corp., Minnesota, USA, 1992.